Geochemical Perspectives Letters

Noble gas incorporation into silicate glasses: implications for planetary volatile storage

H. Yang, A.E. Gleason, S.N. Tkachev, B. Chen, R. Jeanloz, W.L. Mao

Supplementary Information

The Supplementary Information includes:

- Sample Preparation
- Brillouin Spectroscopy Measurements
- Volume Compression Curve Calculation
- Tables S-1 and S-2
- Figures S-1 to S-4
- Supplementary Information References

Sample Preparation

High-purity silica glass was synthesised at Corning Inc. by chemical vapor deposition and was annealed at 985 °C for 1500 hours. Its OH content was determined by FTIR spectroscopy to be 268 (± 7) ppm. Details of the determination of OH content are reported elsewhere (Clark *et al.*, 2014).

Natural Kilauea basalt glass was collected at the Kilauea volcano, Hawaii. The natural sample was prepared by grinding a kilogram sample into a powder and melting at 1540 °C under a nitrogen atmosphere. Two heating-quenching cycles in a furnace ensured a uniform amorphous state (Jochum *et al.*, 2000). X-ray diffraction of the samples after polishing and loading showed no crystalline phases. Chemical analysis of sample was conducted using Electron Probe Micro Analysis, and results are listed in Table S-1.

The synthesised samples were double-sided polished to ~30 um in thickness and loaded into a 200 μm diameter sample chamber drilled into a pre-indented rhenium gasket that was compressed between a pair of 400 μm flat diamond anvils. Ruby spheres were also loaded in the chamber to calibrate pressure. For silica glass, neon was loaded as the pressure medium using the gas loading system at GSECARS, Argonne National Laboratory (ANL) (Rivers *et al.*, 2008). For basalt glass, a methanol-ethanol mixture (M-E mixture) with a 4:1 ratio was used as the pressure medium.

Brillouin Spectroscopy Measurements

Brillouin scattering was performed using two different systems: (1) at the Advanced Light Source, Lawrence Berkeley National Laboratory, and (2) the Advanced Photon Source, Argonne National Laboratory. Brillouin spectra were collected up to 10 GPa for Silica glass in neon, and up to 22 GPa for basalt glass in a M-E mixture at beamline 13-BMD, GSECARS, ANL (Sinogeikin *et al.*, 2006) (Figs.1 and S-1). All measurements were made on compression at room temperature, and at each pressure samples were held for 30 minutes to stabilise pressure before data collection. Both Brillouin systems used a solid-state 532nm laser, and a six-pass tandem Fabry-Perot Interferometer along with a photomultiplier tube. Typical Brillouin spectra collection times were 15 to 30 minutes. Symmetric platelet geometry was used in the measurement to cancel the refractive-index correction in calculating velocities (Whitfield *et al.*, 1976). The *P*- and *S*-wave velocities were derived from the frequency shifts of the incident photons in the Brillouin spectra:

$$V = \frac{\Delta\nu \cdot \lambda}{2sin\frac{\theta}{2}} , \qquad \text{Eq. S-1}$$

where V is the acoustic wave velocity, $\boldsymbol{\Delta\nu}$ is the frequency shift, $\boldsymbol{\lambda}$ is the wavelength of the laser, and θ is the angle between the incident and scattered light. Uncertainties in the velocities were estimated from fitting results for the phonon peak positions (Table S-2).

Volume Compression Curve Calculation

The isentropic bulk modulus K_S can be derived from the velocities, and is related to the derivative of pressure with respect to density:

$$K_S = \rho\left(\frac{\partial P}{\partial \rho}\right)_S = \rho\left(v_P^2 - \frac{4}{3}v_s^2\right) \quad \text{Eq. S-2}$$

Correction from isentropic to isothermal conditions is small at room temperature ($K_S = K_T\,(1 + agT)$, with the product of thermal expansion coefficient a, Grüneisen parameter g and temperature T, being less than 10^{-2}). Therefore, integration of (2) could be used to calculate the volume decrease of the glasses under static compression (subscript T indicates isothermal conditions):

$$\frac{V}{V_0} = \left(\frac{\rho}{\rho_0}\right)_T^{-1} = \left(1 + \frac{1}{\rho_0}\int_{P_0}^{P}\frac{dP}{v_P^2 - \frac{4}{3}v_S^2}\right)_T^{-1} \quad \text{Eq. S-3}$$

except for two significant effects. First, Eq. S-3 ignores any volume change associated with changes in glass structure under compression (measured velocities of crystalline samples can similarly be integrated as a function of pressure, and also do not include the volume change across any crystal-structural phase transition; the volume change on transformation is instead an unknown integration constant). This effect implies that the glass sample should actually undergo greater volume compression than predicted by Eq. S-3, especially as there can in principle be dispersion between the elastic response at Brillouin frequencies and the quasi-static response under isothermal compression.

Second, Eq. S-3 ignores the possibility that the sample is an open system, in that noble gas (pressure medium) is permeating into the glass structure. In this case, we can think of the glass as being a porous medium, with noble gas filling the structural void spaces represented by porosity (*e.g.*, Weigel *et al.*, 2012). If the glass structure can be treated as rigid, filling empty pores is expected to increase the velocities of the medium; in detail, the relationship between volume compression and measured velocities is complex, however, due to potentially competing effects of structural rearrangement and void filling.

Applying the integrated Eq. S-3 to the Brillouin results does indeed produce larger volumes (*i.e.* less compression) as compared with isothermal compression measurements by optical and x-ray tomographic methods for silica and basalt glasses (Fig. S-3). This implies that the glasses undergo structural rearrangement on compression, as expected for instance due to rotation of SiO_4 tetrahedra into void spaces. The effect is relatively small for Silica glass compressed in M-E, however, and the Brillouin measurements document an additional stiffening (larger volumes at high pressure) when Ne or He are used as pressure media. Similarly, the basalt glass in Ne exhibits extra stiffening in the Brillouin velocities relative to static compression in M-E-W. In both cases, we attribute this additional stiffening (higher Brillouin velocities), as compared with M-E, to the incorporation of Ne or He into the glass structure.

Supplementary Tables

Table S-1 Composition of Kilauea Basalt sample from Electron Probe Microanalysis (weight %). The compositions of two other basaltic glasses discussed in the text were also listed for comparison. Abbreviations: KB, Kilauea Basalt; BIR-1, Icelandic Basalt; BCR-2, Columbia River Basalt. NBO/T for KB, BIR-1, and BCR-2 are 0.8, 0.9, and 0.6, respectively. Slight differences among the compositions of these basalt glasses are unlikely to significantly affect the pressure dependences or transition points for the velocities.

Oxide	KB, This study	BIR-1	BCR-2
SiO_2	49.67	47.96	54.1
TiO_2	2.91	0.96	2.26
Al_2O_3	13.49	15.5	13.5
FeO	14.24	10.2	12.4
MnO	0.18	0.175	0.196
MgO	5.94	9.7	3.59
CaO	9.72	13.3	7.12
Na_2O	2.56	1.82	3.16
K_2O	0.69	0.03	1.79

Table S-2 Experimental sound velocity data measured by Brillouin Spectroscopy. A Lorentz function was used to fit the peak and the uncertainties in the velocities were estimated from the fitting results of the phonon peak positions.

Sample	Pressure (GPa)	V_S (km/s)	Uncertainty	V_P (km/s)	Uncertainty
Kilauea basalt glass	0.0	3.53	0.03	6.26	0.03
Kilauea basalt glass	2.4	3.00	0.07	5.85	0.03
Kilauea basalt glass	4.2	3.07	0.11	5.39	0.04
Kilauea basalt glass	11.2	3.49	0.07	6.36	0.03
Kilauea basalt glass	14.3	3.74	0.06	7.13	0.02
Kilauea basalt glass	18.9	4.30	0.12	8.77	0.03
Kilauea basalt glass	22.0	4.11	0.09	8.79	0.04
Kilauea basalt glass	21.3[a]	4.27	0.16	8.91	0.06
Kilauea basalt glass	18.4[a]	4.28	0.08	8.22	0.26
Kilauea basalt glass	16.7[a]	4.04	0.15	8.23	0.04
Kilauea basalt glass	14.8[a]	3.98	0.11	7.60	0.17
Kilauea basalt glass	13.2[a]	3.94	0.11	7.29	0.06
Kilauea basalt glass	11.3[a]	3.77	0.09	7.01	0.03
Kilauea basalt glass	5.9[a]			6.87	0.03
Kilauea basalt glass	3.5[a]			6.54	0.06
Kilauea basalt glass	2.4[a]			6.38	0.06
Silica glass	0.0	3.74	0.02	5.89	0.03
Silica glass	0.8	3.57	0.02	5.71	0.03
Silica glass	1.0	3.56	0.02	5.69	0.03
Silica glass	1.1	3.52	0.01	5.68	0.02
Silica glass	1.3	3.52	0.02	5.69	0.03
Silica glass	1.5	3.52	0.03	5.70	0.02
Silica glass	1.8	3.51	0.03	5.73	0.03
Silica glass	2.0	3.50	0.03	5.74	0.02
Silica glass	2.1	3.49	0.02	5.76	0.03
Silica glass	2.8	3.49	0.03	5.83	0.04
Silica glass	3.5	3.50	0.04	5.91	0.04
Silica glass	4.1	3.52	0.02	6.01	0.03
Silica glass	4.6	3.54	0.02	6.12	0.03
Silica glass	5.9	3.55	0.02	6.15	0.03
Silica glass	7.4	3.57	0.02	6.32	0.04
Silica glass	9.3	3.60	0.02	6.46	0.03
Silica glass	9.4	3.68	0.03	6.71	0.03
Silica glass	10.5			7.25	0.02

[a] data collected during the decompression run.

Supplementary Figures

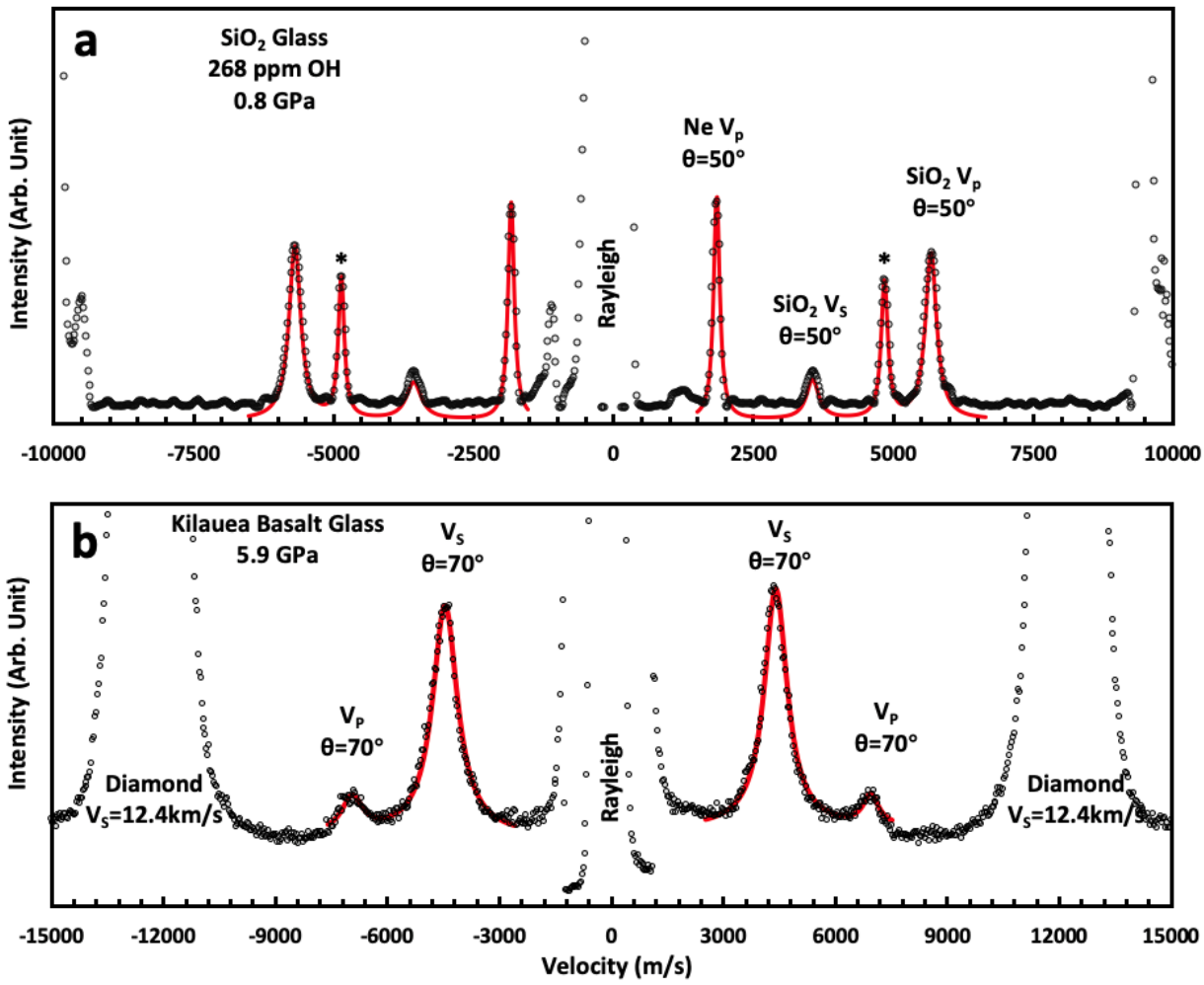

Figure S-1 Representative Brillouin spectra for silica glass at 0.8 GPa and Kilauea basalt glass at 5.9 GPa. Black squares represent raw data while red lines represent Lorentz peak fitting results. At 0.8 GPa, neon is supercritical fluid and only its V_P mode is observed. The Ne back scattering signal marked by * came from the reflected laser on the downstream diamond.

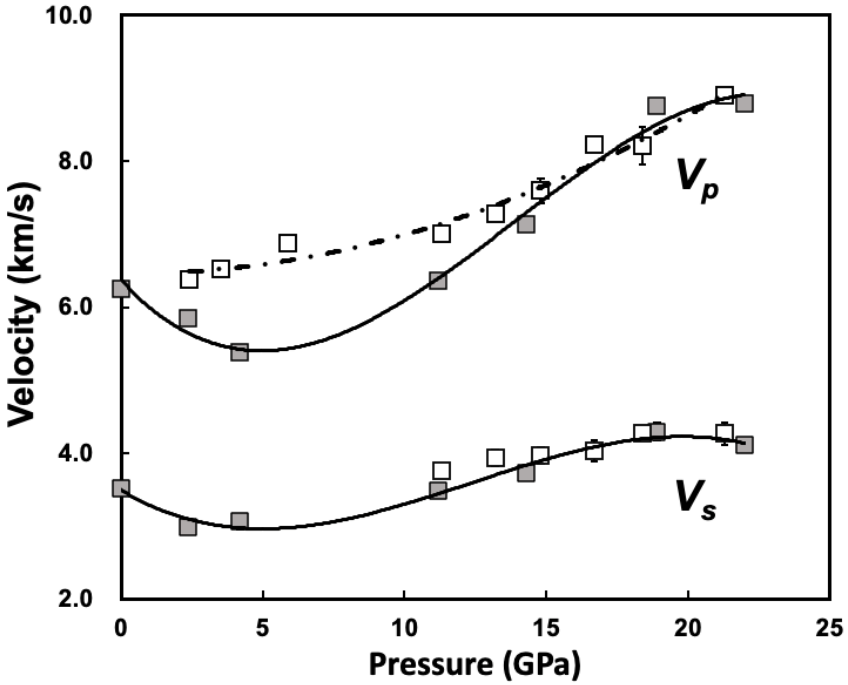

Figure S-2 Compression and decompression measurements of sound velocities of silica glass at high pressure. Filled squares show compression data while open squares show decompression data. Lines are guides for the eye.

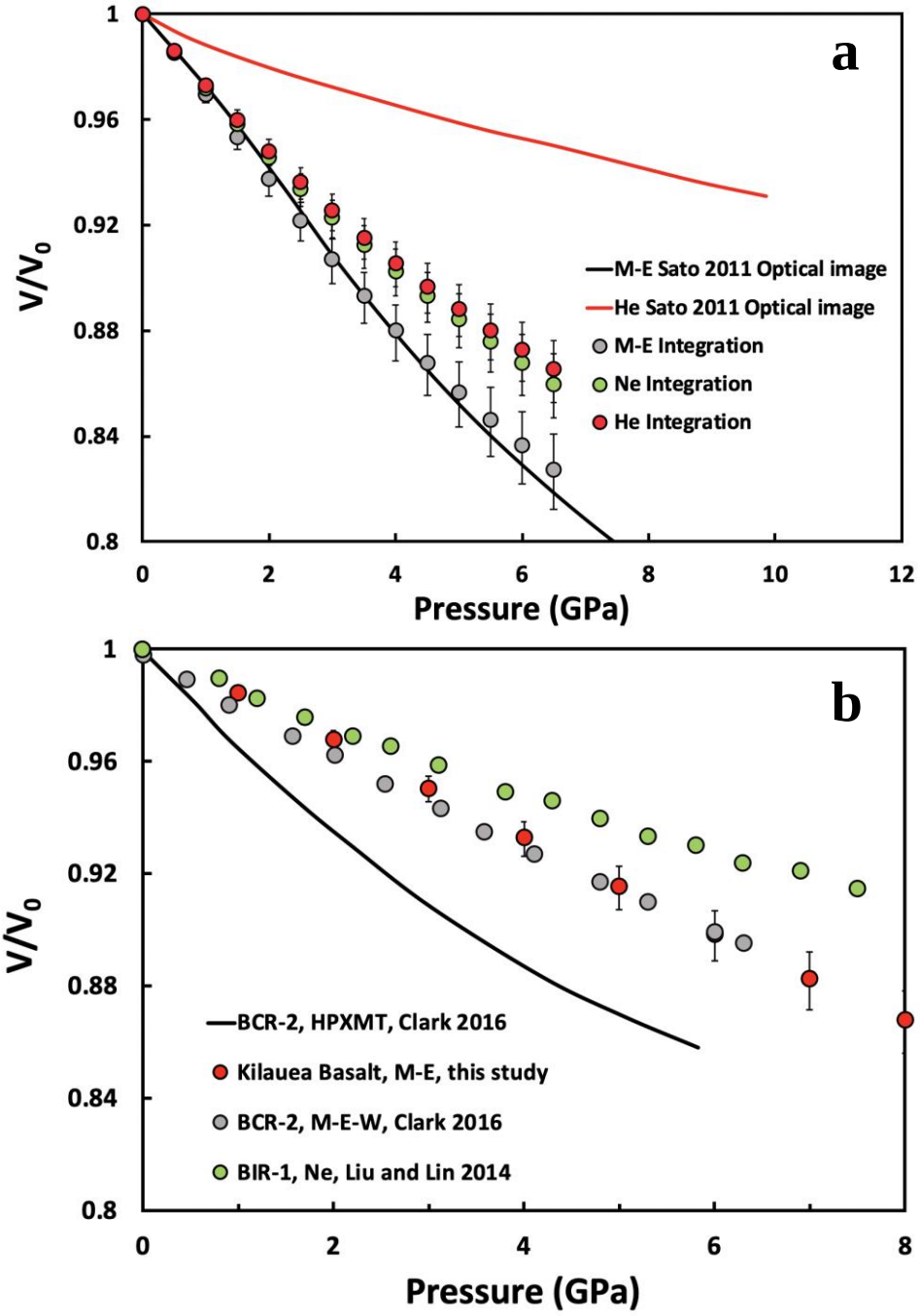

Figure S-3 Relative volume reduction of silica glass and basaltic glasses derived from different methods. M-E-W: 16:3:1 Methanol-Ethanol-Water mixture, M-E: 4:1 Methanol-Ethanol mixture, HPXMT: high-pressure X-ray microtomography. Filled circles are results from bulk sound velocity integration method based on $\frac{V}{V_0} = \left(\frac{\rho}{\rho_0}\right)^{-1} = \left(1 + \frac{1}{\rho_0}\int_{P_0}^{P} \frac{dP}{v_P^2 - \frac{4}{3}v_S^2}\right)^{-1}$ (Eq. S-3). we used a generous ±5% uncertainty in V_S and V_P to calculate the resulting uncertainty in V/V_0. Lines represent results from X-ray tomography (HPXMT) or optical image measurements.

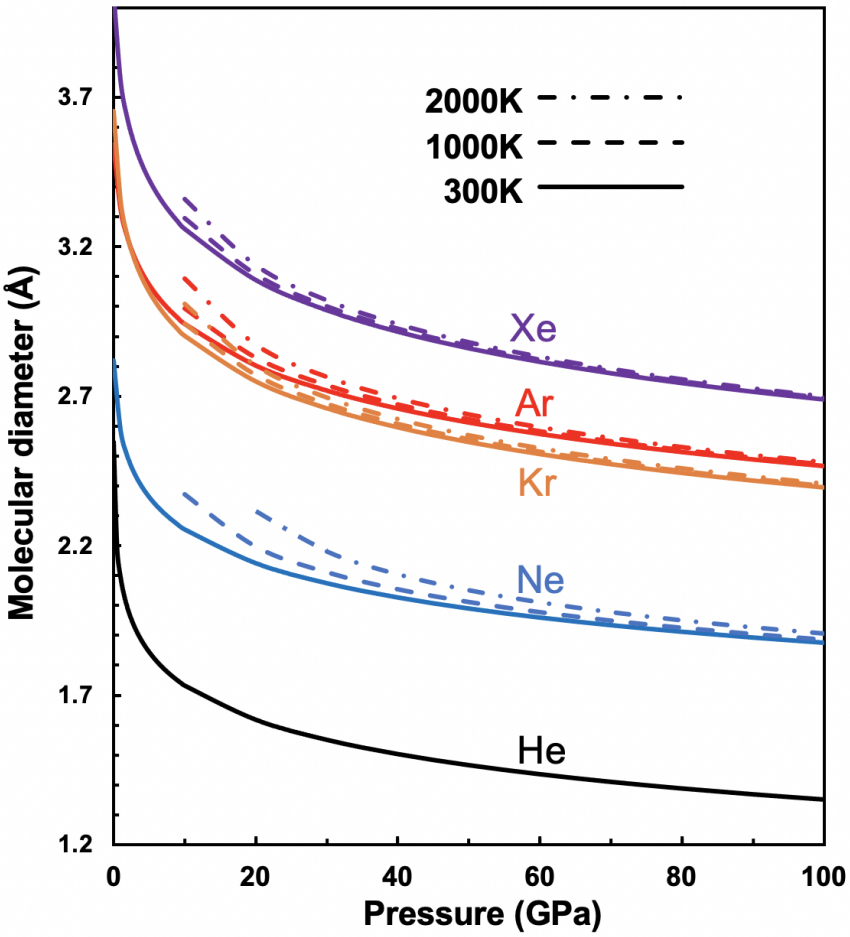

Figure S-4 Molecular size of noble gases as a function of pressure and temperature. Molecular size data at ambient conditions were taken from Reid *et al.* (1987). Thermal EoS data of noble gases were taken from Rosa *et al.* (2020). We did not include the high temperature effect on helium as its thermal EoS above 300 K has not been well established.

Supplementary Information References

Clark, A.N., Lesher, C.E., Jacobsen, S.D., Sen, S. (2014) Mechanisms of anomalous compressibility of vitreous silica. *Physical Review B* 90, 174110.

Clark, A.N., Lesher, C.E., Jacobsen, S.D., Wang, Y. (2016) Anomalous density and elastic properties of basalt at high pressure: Reevaluating of the effect of melt fraction on seismic velocity in the Earth's crust and upper mantle. *Journal of Geophysical Research: Solid Earth* 121, 4232–4248.

Liu, J., Lin, J.-F. (2014) Abnormal acoustic wave velocities in basaltic and (Fe,Al)-bearing silicate glasses at high pressures. *Geophysical Research Letters* 41, 8832–8839.

Jochum, K.P., Dingwell, D.B., Rocholl, A., Stoll, B., Hofmann, A.W., Becker, S., Besmehn, A., Bessette, D., Dietze, H.-J., Dulski, P., Erzinger, J., Hellebrand, E., Hoppe, P., Horn, I., Janssens, K., Jenner, G.A., Klein, M., McDonough, W.F., Maetz, M., Mezger, K., Müker, C., Nikogosian, I.K., Pickhardt, C., Raczek, I., Rhede, D., Seufert, H.M., Simakin, S.G., Sobolev, A.V., Spettel, B., Straub, S., Vincze, L., Wallianos, A., Weckwerth, G., Weyer, S., Wolf, D., Zimmer, M. (2000) The Preparation and Preliminary Characterisation of Eight Geological MPI-DING Reference Glasses for In-Situ Microanalysis. *Geostandards and Geoanalytical Research* 24, 87–133.

Reid, R.C., Prausnitz, J.M., Poling, B.E. (1987) The properties of gases and liquids. McGraw Hill Book Co., New York, NY.

Rivers, M., Prakapenka, V.B., Kubo, A., Pullins, C., Holl, C.M., Jacobsen, S.D. (2008) The COMPRES/GSECARS gas-loading system for diamond anvil cells at the Advanced Photon Source. *High Pressure Research* 28, 273–292.

Rosa, A.D., Bouhifd, M.A., Morard, G., Briggs, R., Garbarino, G., Irifune, T., Mathon, O., Pascarelli, S. (2020) Krypton storage capacity of the Earth's lower mantle. *Earth and Planetary Science Letters* 532, 116032.

Sato, T., Funamori, N., Yagi, T. (2011) Helium penetrates into silica glass and reduces its compressibility. *Nature Communications* 2, 345.

Sinogeikin, S., Bass, J., Prakapenka, V., Lakshtanov, D., Shen, G., Sanchez-Valle, C., Rivers, M. (2006) Brillouin spectrometer interfaced with synchrotron radiation for simultaneous x-ray density and acoustic velocity measurements. *Review of Scientific Instruments* 77, 103905.

Weigel, C., Polian, A., Kint, M., Rufflé, B., Foret, M., Vacher, R. (2012) Vitreous Silica Distends in Helium Gas: Acoustic Versus Static Compressibilities. *Physical Review Letters* 109, 245504.

Whitfield, C.H., Brody, E.M., Bassett, W.A. (1976) Elastic moduli of NaCl by Brillouin scattering at high pressure in a diamond anvil cell. *Review of Scientific Instruments* 47, 942–947.